Science of the Total Environment 843 (2022) 157092

Contents lists available at ScienceDirect

Science of the Total Environment

journal homepage: www.elsevier.com/locate/scitotenv

Unmanned aerial vehicles (UAVs) as a tool for hazard assessment: The 2021 eruption of Cumbre Vieja volcano, La Palma Island (Spain)

A. Román [a,*], A. Tovar-Sánchez [a], D. Roque-Atienza [a], I.E. Huertas [a], I. Caballero [a], E. Fraile-Nuez [b], G. Navarro [a]

[a] Department of Ecology and Coastal Management, Institute of Marine Sciences of Andalusia (ICMAN), Spanish National Research Council (CSIC), 11510 Puerto Real, Spain
[b] Canary Islands Oceanographic Centre, Spanish Institute of Oceanography (IEO), Spanish National Research Council (CSIC), 38180 Santa Cruz de Tenerife, Spain

HIGHLIGHTS

- UAVs provide crucial information for hazard assessment during a volcanic event.
- Feasible tool for accurately elaborate DEMs, 3D models and topographic maps
- Centimeter-scale approximation of the area devastated by the lava flow
- UAV data allowed the performance of lava flow flooding forecasting models.
- Chemical analysis of surface water samples obtained under the influence of the lava delta

GRAPHICAL ABSTRACT

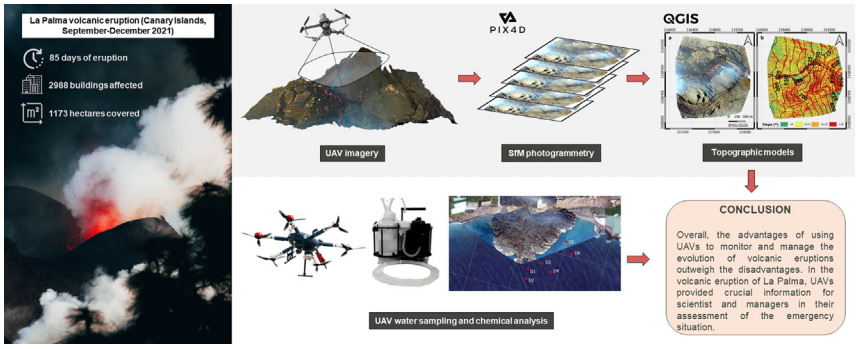

ARTICLE INFO

Editor: Damià Barceló

Keywords:
Unmanned aerial vehicle (UAV)
Volcanic eruptions
Hazard assessment
La Palma eruption
Lava forecasting

ABSTRACT

Monitoring for assessment of natural disasters, such as volcanic eruptions, presents a methodological challenge for the scientific community. Here, we present Unmanned Aerial Vehicles (UAVs) as a feasible, precise, rapid and safe tool for real time monitoring of the impacts of a volcanic event during the Cumbre Vieja eruption on La Palma Island, Spain (2021). UAV surveys with optical RGB (Red-Green-Blue), thermal and multispectral sensors, and a water sampling device, were carried out in different areas affected by the lava flow, including the upper volcanic edifice and the lava delta formed on the coastal fringe of the island. Our results have provided useful information for the monitoring of the advance of the lava flow and its environmental consequences during the volcanic emergency. Our data shows how La Palma island's growth, with the formation of a new lava delta of 28 ha and a total volume of lava injected into the sea of 5,138,852 m^3. Moreover, our Digital Elevation Model (DEM) simulated, with a 70 % accuracy, the probabilistic simulation of the possible path followed by the lava flow in the vicinity of the fissure from which the magma emanates. In addition, significant changes of seawater physical-chemical parameters were registered in coastal surface waters by the *in situ* seawater samples collected with the automatic water sampling device of our UAV. The first meters of the water column, due to the instant evaporation of the seawater in contact with the hot lava, produce an increase of temperature and salinity of up to 4–5 °C and up to 5 units, respectively.

1. Introduction

A natural disaster constitutes a dynamic scenario, which is complicated to manage and has negative impacts on the natural environment, economy and society (Colson et al., 2018; Dou et al., 2014; Giordan et al., 2018). Consequently, a large number of people are affected by natural disasters in both developing and developed economies (Giordan et al., 2018; Krapivin et al., 2012; Kucharczyk and Hugenholtz, 2021; Sukov et al., 2008). For this reason, suitable methodologies are essential in order to evaluate the impact of these phenomena and in particular to monitor their evolution in real time in order to help decision makers minimize and/or mitigate the damages

* Corresponding author.
E-mail address: a.roman@csic.es (A. Román).

http://dx.doi.org/10.1016/j.scitotenv.2022.157092
Received 10 May 2022; Received in revised form 8 June 2022; Accepted 27 June 2022
Available online 30 June 2022

during emergencies (Cracknell and Varotsos, 2011; Giordan et al., 2018). The use of satellite imagery for the monitoring of natural disasters has become a common practice, since satellites operate continuously covering wide areas with medium-high spatial resolution (Ganci et al., 2020; Solikhin et al., 2012). The application of remote sensing satellite imagery for natural disasters began around 2000 by the International Charter Space and Major Disasters and the United Nations (UN) (Bessis et al., 2004; Kaku, 2019). Nowadays, global emergency agencies using satellite-based monitoring support the management of natural disasters by providing geospatial information derived from optical instruments, thermal sensors, altimetry systems, synthetic aperture radar (SAR), Laser Imaging Detection and Ranging (LiDAR), radiometers and spectrometers (Borgeaud et al., 2015; Colson et al., 2018). In particular, these agencies include the United States Geological Surveys (USGS) Emergency Response (Fink et al., 1990; Mueller et al., 2015), the Asia-Pacific Regional Space Agency Forum (APRSAF) Sentinel Asia (Adriano et al., 2019; Kaku, 2019), or the Copernicus Emergency Management Service (CEMS) (Copernicus Emergency Management Service, n.d.), whose space segment is made up of five Sentinel satellites that allow the monitoring of floods (DeVries et al., 2020; Konapala et al., 2021; Yuan et al., 2021), earthquakes (Jelének and Kopacková-Strnadová, 2021; Li et al., 2021), harmful algal blooms (Caballero et al., 2020; Ogashawara, 2019; Rodríguez-Benito et al., 2020), wildfires (Ban et al., 2020; Colson et al., 2018; Llorens et al., 2021) and volcanic eruptions (Bell et al., 2021; Coca et al., 2014; Gray et al., 2019; Plank et al., 2020), among others.

Volcanic eruptions are hazardous and particularly challenging for ground-data collection or direct observations (Walter et al., 2020), and require remote sensing tools for their monitoring and risk assessment. However, applicability of satellite remote sensing in the study of volcanic events remains limited because of the reliance on optimal meteorological conditions and the consequent unavailability of observations for specific dates and locations (Andaru et al., 2021; Bonali et al., 2019), with the exception of those equipped with thermal and radar sensors (*e.g.* SAR), which can work at night, with cloud cover, *etc.* In addition, despite the advances in satellite remote sensing technology, it is still difficult to monitor these dynamic phenomena due to their coarse spatial image resolution and their long re-acquisition intervals (Turner et al., 2017). To overcome these limitations, the use of different sensors mounted on Unmanned Aerial Vehicles (UAVs) for the monitoring of volcanic eruptions is gaining prominence as a complement to satellite remote sensing (Andaru et al., 2021; Pering et al., 2020; Zorn et al., 2020). There are few studies that have employed UAVs in the assessment of volcanic eruptions assessment to: evaluate their geomorphological description and elaborate digital terrain models (Darmawan et al., 2018; Favalli et al., 2018; Walter et al., 2020); measure the volcanic gas composition of the ash column (Kazahaya et al., 2019; Liu et al., 2019; Mori et al., 2016); analyze the lava flow characteristics and develop models that allow the prediction of their behavior (Dietterich et al., 2017; Turner et al., 2017); or sample water at crater lakes (Terada et al., 2018).

UAVs offer an alternative to overcome the main limitations of other remote sensing techniques such as satellites during volcanic crises, since: i) they provide topographic data with centimeter spatial resolution; ii) they allow better control of temporal resolution, increasing the flexibility for image/video acquisition or water/gas sampling; iii) their operation is not limited by the presence of volcanic ash within eruption columns; iv) they reduce human risk during data collection in the field, particularly in difficult, restricted or dangerous areas; v) multiple parameters can be measured with different devices or sensors (thermal, hyperspectral, multispectral, RGB, LiDAR, gas detector, water sampling device); and vi) they are able to obtain results in real time facilitating the topographic modeling and lava flow dynamics for hazard evaluation (Giordan et al., 2018; Gomez and Purdie, 2016; Turner et al., 2017).

Here, we present the La Palma volcanic eruption (Canary Islands, Spain) as our case study (Fig. 1). The new eruption on the Cumbre Vieja ridge, started on September 19th 2021 from multiple vents aligned in a single linear fissure segment in the Earth's crust, emitting (inland and towards the ocean) large amounts of lava and volcanic material during the eruption period. The eruption was officially declared finalized on December 25th 2021, after three months of spewing ash and hot molten rock. Volcanic eruptions directly affect people living on or near the volcano, who are forced to be evacuated due to: i) ash fallout, that may cause building collapse as a result of rapid accumulation and high density of volcanic ash particles; ii) toxic gases (SO_2, H_2S) which may pose respiratory health risks; or iii) direct effect of lava flow destroying numerous hectares of cultivated land and buildings (Malawani et al., 2021). In addition, lava flows from the eruption can lead to geomorphological transformations in the volcano edifice due to erosion and sedimentation processes, and they have a significant impact on water bodies (including lakes, reservoirs or the ocean) since they affect water quality, generate harmful gases on contact with water, or even create small tsunamis (Malawani et al., 2021; Stewart et al., 2006). In order to monitor the impacts and environmental processes occurring during the eruption, we used two UAVs equipped with different sensors, as well as a water sampling device (see Methods section), to provide real time data of the evolution of the volcanic activity. We elaborated Digital Elevation Models (DEMs), orthophotos and 3D models from structure from motion (SfM) photogrammetry during three eruption days, allowing us to analyze the morphology of sub-meter-scale volcanic features over kilometer-scale areas; to detect temperature anomalies that can be indicative of magmatic activity; to explore the lava flow path and characteristics in order to contribute to hazard assessment; and to determine the impact of the magma on the ocean. The survey also aims to provide precise data for emergency teams and authorities for the management of the effects caused by the eruption in real time, highlighting the potential of UAV technology to rapidly obtain high-spatial-resolution data during volcanic crises.

2. Methods

2.1. Study area

During the fieldwork on October 1st-3rd 2021, three different areas of the Cumbre Vieja volcanic eruption on La Palma Island (28°40′0.01″N, 17°52′0.01″W) were surveyed in order to acquire visible, multispectral and thermal imagery using different sensors on board UAVs, as well as surface water samples (Fig. 1). The first two monitored areas were close to the fissures from which the magma emanated to the surface (vent region), corresponding to the upper region of the lava flows (Fig. 1d, e). The third monitored area corresponds to the lava delta formed on the coast of Tazacorte (Fig. 1c). The volcano erupted on September 19th 2021 with a fissural-type eruption, and the lava reached the sea ten days later. Approximately 700 buildings were destroyed by the lava flow according to the data provided by the Council of La Palma (Council of La Palma, n.d.) and the Copernicus Emergency Management Service (CEMS) (Copernicus Emergency Management Service, n.d.) during the flight date. Nevertheless, and due to the continuous advance of the lava, the total number of destroyed buildings continued rising every day, reaching a total of 2988 buildings covered by the flow at the end of the eruption (Copernicus Emergency Management Service, n.d.). After 85 days of eruption, December 25th 2021 was considered the end of the volcanic event, the longest eruption recorded in the history of the island (IGN, 2021).

2.2. Sentinel-2 imagery

The Sentinel-2 twin polar-orbiting satellites developed by the European Commission (EC) and the European Space Agency (ESA) were also used in this study. The multispectral instruments (MSI) on-board both satellites are now operational with a global 5-day revisit frequency at the equator. The MSI samples 13 spectral bands: four bands at 10 m, six bands at 20 m and three bands at 60 m spatial resolution. Detailed information about the radiometric and spectral characteristics of the visible and near-infrared (NIR) bands are specified in the User Handbook (ESA, 2015, 2017). The Sentinel-2 Level-2A surface reflectance products (corrected from the

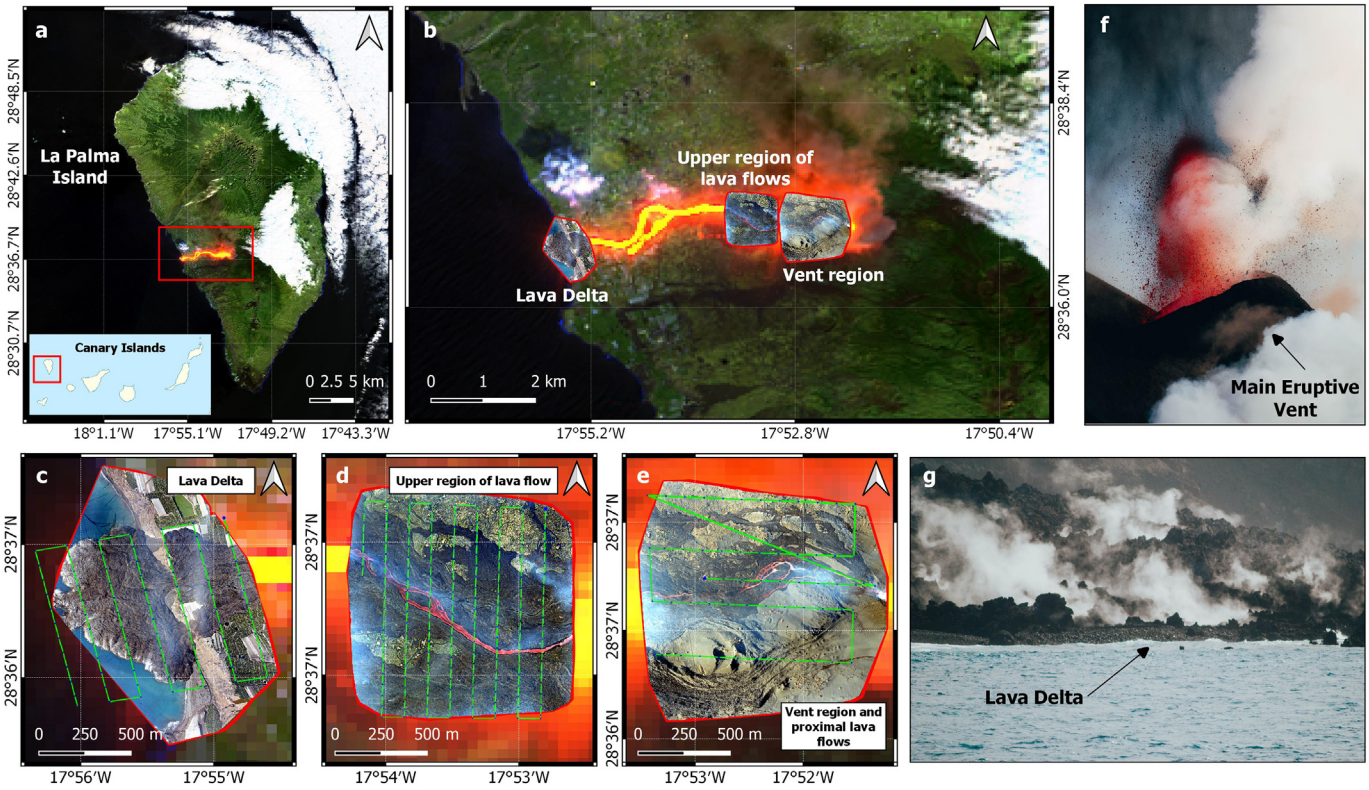

Fig. 1. a) Sentinel-2 level 2A false color (urban) composite (bands 12, 11, 4) from September 30th 2021, with b) detailed representation of the three volcano areas covered in this study. Flight plans over c) the lava delta formed over the sea, d) the upper region of lava flows and e) the vent region and the adjacent lava flows in the flank of the cone. Pictures of f) the main eruptive vent and g) the lava delta taken October 1st 2021. The QGIS software (v.3.16.14, https://qgis.org/downloads/) was used to create the figures.

atmospheric effects) at 10 m spatial resolution used in this study corresponded to the September 10th 2021 and the October 15th 2021 scenes (tile 28RBS).

2.3. UAV platforms and sensors

In this study, two UAVs were used:

1) A hexacopter with three-bladed propellers (Condor, Dronetools ©), which has a DJI6010 electric motor powered by four Li-ion batteries (7000 mA each). The empty weight of the equipment with the four batteries is 11.8 kg (maximum takeoff weight (MTOW) is 14.9 kg), with maximum flight autonomy of up to 60 min (without payload). This UAV was simultaneously equipped with a MicaSense RedEdge-MX dual multispectral camera and the radiometric thermal camera FLIR Vue Pro 19 mm. The multispectral camera has 10 different spectral bands able to acquire data in the following wavelengths: coastal blue 444 nm, blue 475 nm, green 531 and 560 nm, red 650 and 668 nm, red edge 705, 717 and 740 nm, and near infrared (NIR) 842 nm. In addition, the camera allows a broad surface coverage since it has a horizontal field of view of 47.2°, and a spatial resolution of 8 cm/pixel from 120 m high. It also has a Downwelling Light Sensor (DLS) with built-in GPS providing more accurate and reliable measurements of irradiance and solar angle, and the included calibration panel (RP04-1924106-0B) for improved radiometric calibration. The thermal camera captures non-contact temperature measurements with calibrated temperature data embedded in every pixel, its spectral band is 7.5–13.5 μm and it has a sensor resolution of 336 × 256. In addition, this UAV was equipped with a water sampling device (Sparaventi et al., 2022) with an acid cleaned plastic weighted container (2 L) and a castable instrument hanging from the UAV with a 5-meter rope providing instantaneous profiles of temperature and salinity (CastAway^{R}-CTD) and collected surface water.
2) A quadcopter DJI Mavic 2 Pro with an RGB Hasselbald L1D-20c camera with 1" CMOS and 20 MP. Weighing 907 g, it has a maximum flight autonomy of 31 min, which is usually the limiting factor when flying over large areas.

2.4. UAV operations

The flights were preprogrammed using the software DJI Ground Station Pro (GSP), after verifying that weather conditions were favorable for the flight and considering geographical factors, such as the elevation of the terrain. Constant parameters were previously established, including flight height, flight speed, flight time, ground sampling distance (GSD), the trajectory of the UAV and the overlaps (always 80 % frontlap and 70 % sidelap). The multispectral sensor was calibrated, before and after the flight, using a referenced reflectance panel. The Spanish civil aviation regulations for an emergency situation, for which the Spanish Agency for Aviation Safety (AESA) is responsible, were followed during all operations deployed on the ground. All UAV operations of this campaign were carried out between October 1st and 3rd 2021.

The software Pix4D Mapper (Pix4D © SA, Lausanne, Switzerland, v.4.6.4, https://www.pix4d.com/) was used for the SfM photogrammetry. Once the images were imported into the software, different processing steps were performed, including the conversion of digital numbers into relative temperature (°C) for thermal imagery, the generation of the point cloud, the generation of the textured 3D mesh, where obtained 3D points are interpolated to form a triangulated irregular network in order to obtain Digital Elevation Model (DEM). This DEM is then used to project every image pixel and to calculate the georeferenced orthomosaic. The photogrammetric products generated were: i) a 15.7 cm/pixel orthomosaic, a 15.7 cm DEM and a 3D model composed of 60 photos taken at the lava flows adjacent to the vent region at 400 m altitude by an optical RGB sensor (DJI Mavic 2 Pro); ii) a 8.8 cm/pixel orthomosaic and a 9 cm DEM resulting from 176 photos taken at the upper part of the lava flows by an optical RGB

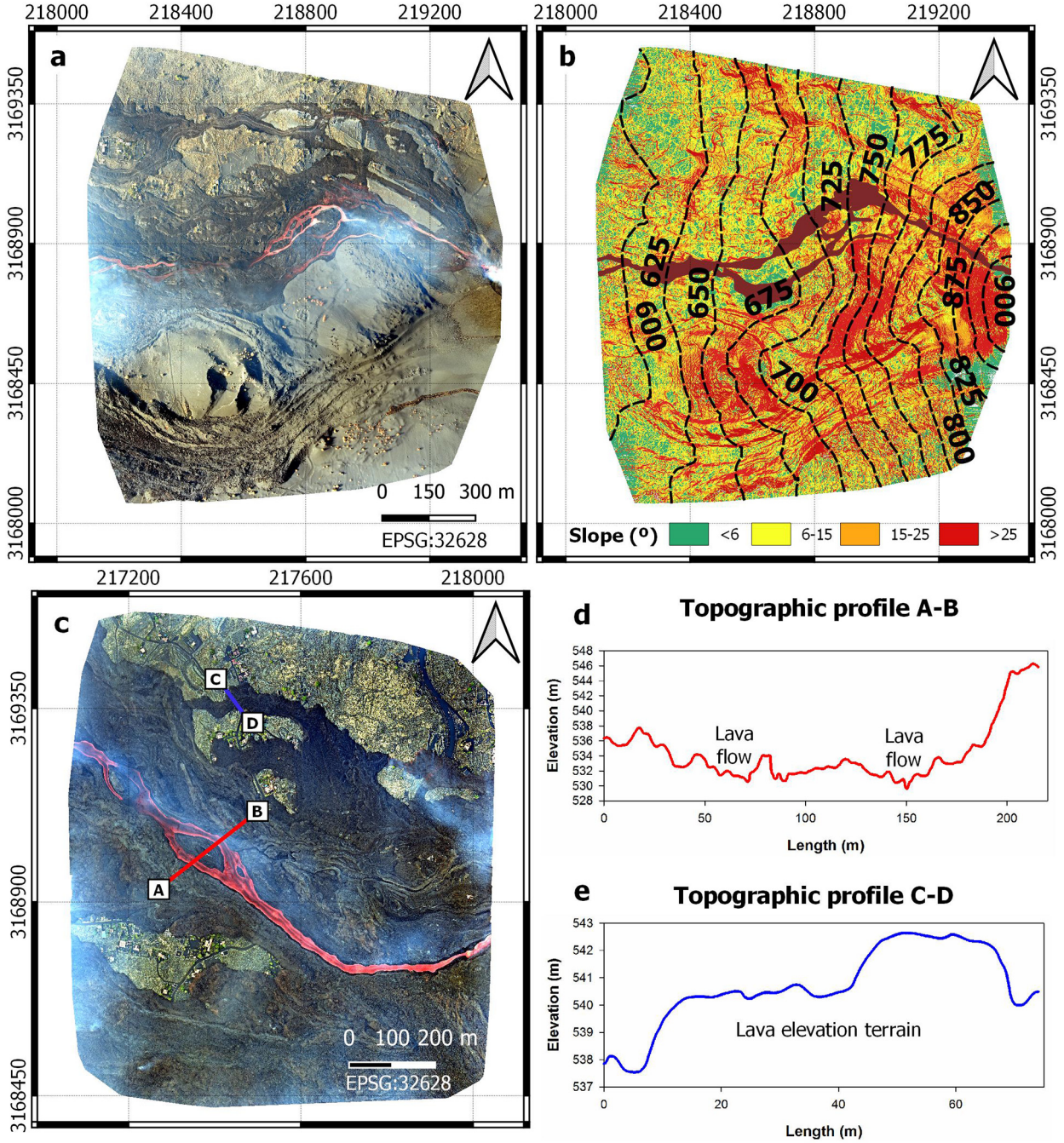
a
b
c
d
e
f
218000
218400
218800
219200
3169350
3168900
3168450
3168000
0 150 300 m
EPSG:32628
Slope (°)
<6
6-15
15-25
>25
600
625
650
675
700
725
750
775
800
825
850
875
900
217200
217600
218000
A
B
C
D
0 100 200 m
Topographic profile A-B
Elevation (m)
Length (m)
Lava flow
Lava flow
Topographic profile C-D
Lava elevation terrain

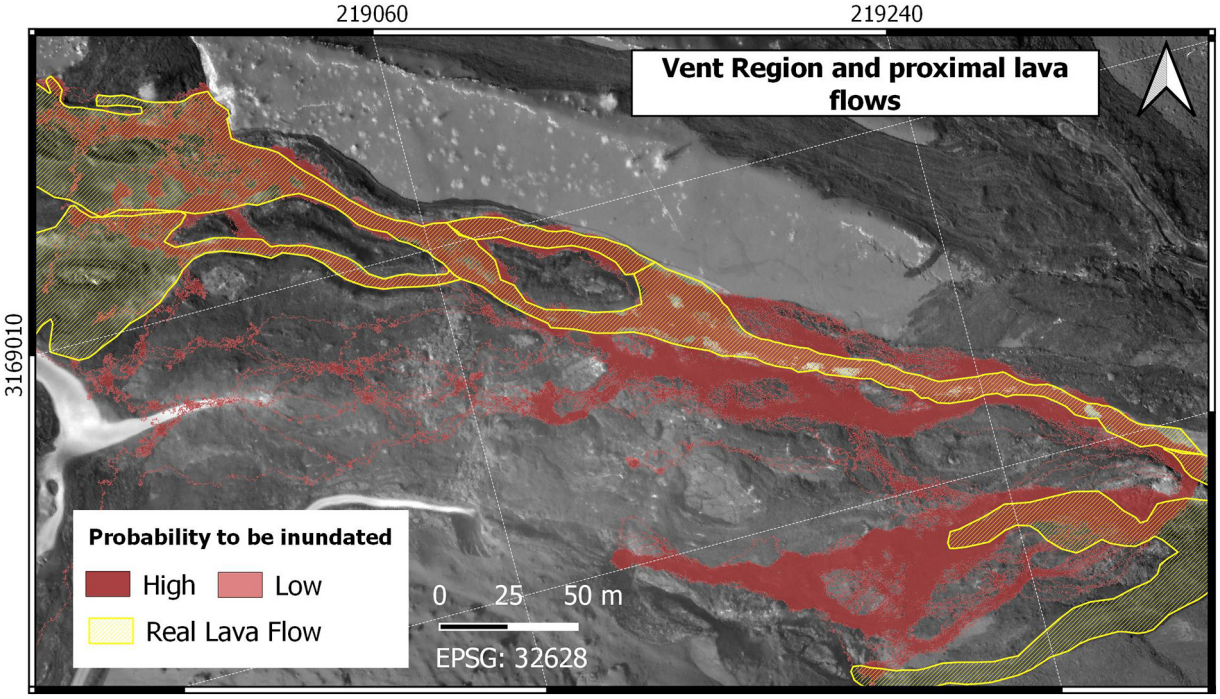

Fig. 3. Lava flow simulation in the vent region and adjacent lava flows in the flank of the cone with the Q-LavHA model from the DEM produced with the UAV flight on October 3rd 2021. The model prediction is shown in red scale, while the real lava flow is shown in yellow. The QGIS software (v.3.16.14, https://qgis.org/downloads/) was used to create the figure.

sensor (DJI Mavic 2 Pro) in a 300 m altitude flight; iii) a 3D model and a 253 photo orthomosaic of 11.8 cm/pixel resolution generated from three optical RGB flights (DJI Mavic 2 Pro) repeated with different gimbal angles (60° and 90°) at a constant height of 300 m over the lava delta; and iv) an orthomosaic of 25.2 cm/pixel derived from 357 thermal captures and an orthomosaic of 20.7 cm/pixel for each of the 10 multispectral bands from a total of 3430 photos taken at the lava delta at 200 m altitude.

Finally, the QGIS (QGIS Development Team, Geographic Information System, Open Source Geospatial Foundation Project, v.3.16.14, https://qgis.org) and SAGA GIS (Conrad et al., 2015, v.7.9.0, https://saga-gis.sourceforge.io/en/index.html) programmes were used to generate topographic models and for their subsequent analysis. Fig. 1 was generated based on the georeferenced information derived from the UAV orthomosaics and the flight plan point clouds obtained from Pix4D processing. The information provided by the DEMs generated from the UAV flights, allowed the elaboration of topographic maps in QGIS using the "slope" raster analysis tool (Fig. 2), and the raster calculator to measure surface areas and volumes (Fig. 4). Quantum-Lava Hazard Assessment (Q-LavHA) was the QGIS plugin used for the lava flow invasion probability simulation (Fig. 3). It combines existing probabilistic and deterministic models (Felpeto et al., 2001; Harris and Rowland, 2001) and proposes some improvements to calculate the probability of lava flow spatial propagation and terminal length. The established parameters for the simulation execution were obtained from the DEMs elaborated with the UAV flights. Specifically, the DEMs themselves, the geographic locations (in UTM) of the volcanic vents, and topographic data such as the value of the elevation in the pixel where the lava flow runs were used. Image classification (Fig. 5) was performed with the supervised classification technique "support vector machine" (SVM), a machine learning algorithm that can successfully handle data with unknown statistical distributions and with small training sets created from spectral data and validated with *in-situ* information (Vapnick, 1995). This approach applies kernel functions that map the training data into a larger-dimensional space in which classes can be linearly separated by a hyperplane. In this case study, the radial base function was used as the transformation nucleus, since it offers the best results as reported by Miranda et al. (2020). Four different land cover classes were created based on the spectral information obtained from vegetation, water, lava flow and any element other than the three previous classes, respectively. The QGIS raster calculator and the SCP (Semiautomatic Classification Plugin) were used for UAV band composites and index generation (NDVI) in Fig. 5.

2.5. Chemical analysis

Total alkalinity (TA) was determined by titration of seawater using a potentiometric system (Mintrop et al., 2002) with a Metrohm 794 Titroprocessor. Water samples were taken directly from the water sampling device and stored in 500 mL borosilicate bottles and poisoned with 100 μL of a saturated aqueous solution of mercuric chloride for later shore-based analysis. The accuracy of the TA determinations was assessed by measurements of Certified Reference Material (CRM batch # 186, supplied by Prof. Andrew Dickson, Scripps Institution of Oceanography, La Jolla, CA, USA), being ±0,06 μmol/kg. Seawater pH was measured using a Metrohm 780 pH meter equipped with a combined glass electrode (Metrohm model 6.0258.010) that included a temperature probe, which was calibrated following the protocol described by Del Valls and Dickson (1998), with an accuracy of ±0.004 pH units. The pH values were then obtained in SWS scale and subsequently transformed to total scale and referred to the *in-situ* temperature (pH_T) using the CO2sys.xls programme (Lewis et al., 1998). The partial pressure of CO_2, pCO_2, was also computed afterwards using the

Fig. 2. Topographic models generated with the SfM workflow followed for the DJI Mavic 2 Pro flight performed on October 1st (at constant 300 m altitude) and 3rd (at constant 400 m altitude) 2021. a) Optical RGB orthomosaic of the vent region and the proximal lava flows in the flank of the cone; b) slope map containing contour lines between 600 and 900 m altitude every 25 m, and the slope expressed in °; c) optical RGB orthomosaic of the upper region of lava flows; d) 225 m topographic profile A–B showing the effect of A'a-type lava flow on the terrain; e) 80 m topographic profile C–D showing the effect of Pahoehoe-type lava flow on the terrain; f) 3D model of the volcanic structure. The QGIS software (v.3.16.14, https://qgis.org/downloads/) was used to create the figures.

pair pH_T, TA values, and proper dissociation constants (Dickson and Millero, 1987; Mehrbach et al., 1973). Seawater samples for the determination of DOC and TDN were collected in 0.25 L acid–cleaned glass bottles and immediately filtered through precombusted (450 °C, 4 h) Whatman GF/F filters with an acid-cleaned all glass filtration system. Aliquots of 20 mL were collected for DOC analysis in precombusted (450 °C, 12 h) 24 mL glass vials. After acidification with H3PO4 (85 %) to pH < 2, they were sealed with Teflon-lined caps and stored in the dark at 4 °C until analyzed in the shore-based laboratory within 1 week of collection. DOC content in samples was measured with a commercial Shimadzu TOCL/CPH/CPN organic carbon analyzer working under the principle of high-temperature catalytic oxidation (Salgado and Miller, 1998). The precision of the analyzer was ±0.5 μmol L^{-1}. Accuracy of measurements was checked with CRM provided by D. A. Hansell (University of Miami, USA), resulting in ±1.3 and −1.8 for DOC and TDN, respectively.

3. Results

DEMs obtained with UAV photogrammetry are essential to assess the lava flow morphology and to obtain several parameters used for flow modeling in the vicinity of the volcanic vent. Lava flows are fundamentally gravity currents that are modulated by internal factors such as viscosity or inflation rates, and by external factors such as slope, terrain roughness or other topographical elements (DeGraffenried et al., 2021; Gomez and Purdie, 2016; Turner et al., 2017). Slope plays a critical role in controlling lava flow behavior, as steeper slope drives advance rates, while topographical features can plug or slow flows (Gomez and Purdie, 2016). Pahoehoe-type lava flows generally move slower than A'a-type flows due to their high density and thickness, although they can cover larger areas (Turner et al., 2017). In the La Palma eruption, the lava flow from the volcano was mainly of A'a-type and Pahoehoe-type (IGN, 2021), as visually observed in the photographs taken *in-situ* and in video footage that shows how the lava flows through the upper flank of the cone (see Supplementary Movie 1 file).

Fig. 2 shows the topographic products resulting from the DEM analysis, which allowed the elaboration of optical RGB orthomosaics (Fig. 2a–c), a slope map with contour lines (Fig. 2b), topographic profiles (Fig. 2d–e), and a 3D model (Fig. 2f) that would allow visual confirmation of the values indicated on the slope map. These products allowed us to obtain valuable parameters for lava flow modeling, such as the slope or terrain elevation, and information on the pathway followed by the lava flow, with a visible decrease of the ground cone from 900 m to 600 m altitude. Similarly, the topographic profile A–B (Fig. 2d) indicates an elevation of approximately 2 m corresponding to the A'a-type lava flow, while the topographic profile C–D (Fig. 2e) shows the elevation of the terrain associated with the accumulation of high density rubbly Pahoehoe-type lava materials, which in some areas reached a height of 12 m. The slope map reflects a more abrupt and irregularly lobulated morphology with slopes between 6° and 15°. The highest slopes were found around the vent region, with approximate values of 25°.

A simple probabilistic flow model (Quantum-Lava Hazard Assessment, Q-LavHA) was generated in order to predict possible lava flow paths and to provide flow hazard assessments (see Methods section). In this case, the DEM obtained during the volcanic event of the most proximal area to the vents through which the lava flow runs, was used. Therefore, it is possible to compare the prediction with real data of the trajectory followed by the lava flow, and demonstrate how these data help predict the most likely lava pathway, thus facilitating prevention and protection activities for emergency services. Fig. 3 shows the areas with the highest probability of flooding due to lava flow, based on the simulation carried out by the Q-LavHA probabilistic model for QGIS. There is a correspondence of over 70 % between the real trajectory followed by the lava flow and the model prediction.

An A'a-type lava delta was formed on the west cliff of the island, near the municipality of Tazacorte. A lava delta is a fan-shaped accumulation of lava flow materials that occurs when the magma that comes into contact with seawater rapidly solidifies, growing in size as volcanic material is accumulated (Bosman et al., 2014; Di Traglia et al., 2018; Zhao et al., 2020). In addition, seawater boils when interacting with lava, generating a toxic column of water vapor, hydrochloric acid and pyroclastics that can reach heights and distances of tens of meters (Hildenbrand et al., 2012; Poland and Orr, 2014). The importance of the study of lava deltas lies not only in the topographic modification of the total surface of the volcanic island (which is increased), but also in its instability since its composition and morphology favor catastrophic collapse that can generate coastal explosions of hurl rocks and fine ash, or even small tsunamis (Bosman et al., 2014; Poland and Orr, 2014). Fig. 4a–b shows the change in the coastline that took place after the formation of the A'a-type lava delta, with a true color composite of Sentinel-2 Level 2A pre-eruption (September 10th 2021) and another false color composite post-eruption (October 15th 2021). The 3D model (Fig. 4c) and optical RGB orthomosaic (Fig. 4d) of the lava delta's main body, allowed the determination of 28 ha (Fig. 4e) over the ocean on October 2nd 2021, and was characterized by an overall lobate morphology with slope gradients between 20°–40°. However, the delta continued growing until it reached approximately 33 ha on October 15th 2021, remaining stable according to the data provided by the CEMS (Copernicus Emergency Management Service, n.d.). It is also evident that there was a higher accumulation of lava at the falling surface of the cliff with abrupt lobes being observed on the flanks, leaving a short steep slope inside the main delta body that rises a few meters above sea level. The DEM analysis allowed us to obtain an approximate total volume of 5,138,852 m^3 in the lava delta, this accumulation being larger in the 4 ha closest to the magma fall at the edge of the cliff, with a volume of 297,220 m^3.

In addition, a photogrammetric flight was carried out in this area with an UAV equipped simultaneously with thermal and multispectral sensors (see Methods section). The thermal map (Fig. 5a) shows the relative temperature changes of the lava flow, colder in the area of the lava delta where it solidified after contact with seawater, and much hotter (the thermal sensor saturates above 150 °C) on the cliff. The false color composite (near infrared (NIR) 840 nm, green 560 nm and red 668 nm bands) and the Normalized Different Vegetation Index (NDVI) (Fig. 5b–c, respectively) show the presence of banana plantations in the area affected by the volcanic activity, which is the most important economic activity on the island. A supervised classification (Fig. 5d) in four ground cover classes was carried out using the "Support Vector Machine" (SVM) method (Vapnick, 1995, see the Methods section), with an overall classification accuracy of 92.07 % and a Cohen's Kappa Index of 0.88 (see uncertainties and error matrix in Supplementary Files Section, Table A). The thematic map shows that 17 ha of banana plantations of the 35 ha identified by Sentinel-2 data (Fig. 4a), were razed to the ground by the lava in the study area.

The volcanic eruption has not only severely impacted buildings and infrastructure of the island, but also the marine environment, with physical-chemical and biological alterations of coastal seawater, which can affect fisheries, that contribute significantly to the island's economy. It is well known that volcanic events provoke explosions generated by thermohydraulic reactions, involving high rates of heat transfer between lava and seawater, and chemical reactions, and the release of huge amounts of metals and gases, mainly Fe, Cu, Cd, Hg and chlorine (with small amounts of sulfur species) that alter the chemistry of seawater (James et al., 2020; Mason et al., 2021). The water sampling device mounted on board the UAV (Tovar-Sánchez et al., 2021, see Methods section) allowed the collection of surface water samples in the areas adjacent to the lava delta, located inside a 500 m security navigation perimeter established by the authorities and, therefore, not accessible by vessels.

Fig. 6 shows temperature and salinity profiles that were obtained at six stations located in the vicinity of the lava delta. The results obtained for the first seven meters of the water column reveal a temperature rise (up to 4–5 °C) and a salinity increase (up to five units) in the first meter due to the instant effect of the hot lava on the colder ocean and the instant evaporation of the seawater, respectively. These important thermohaline anomalies

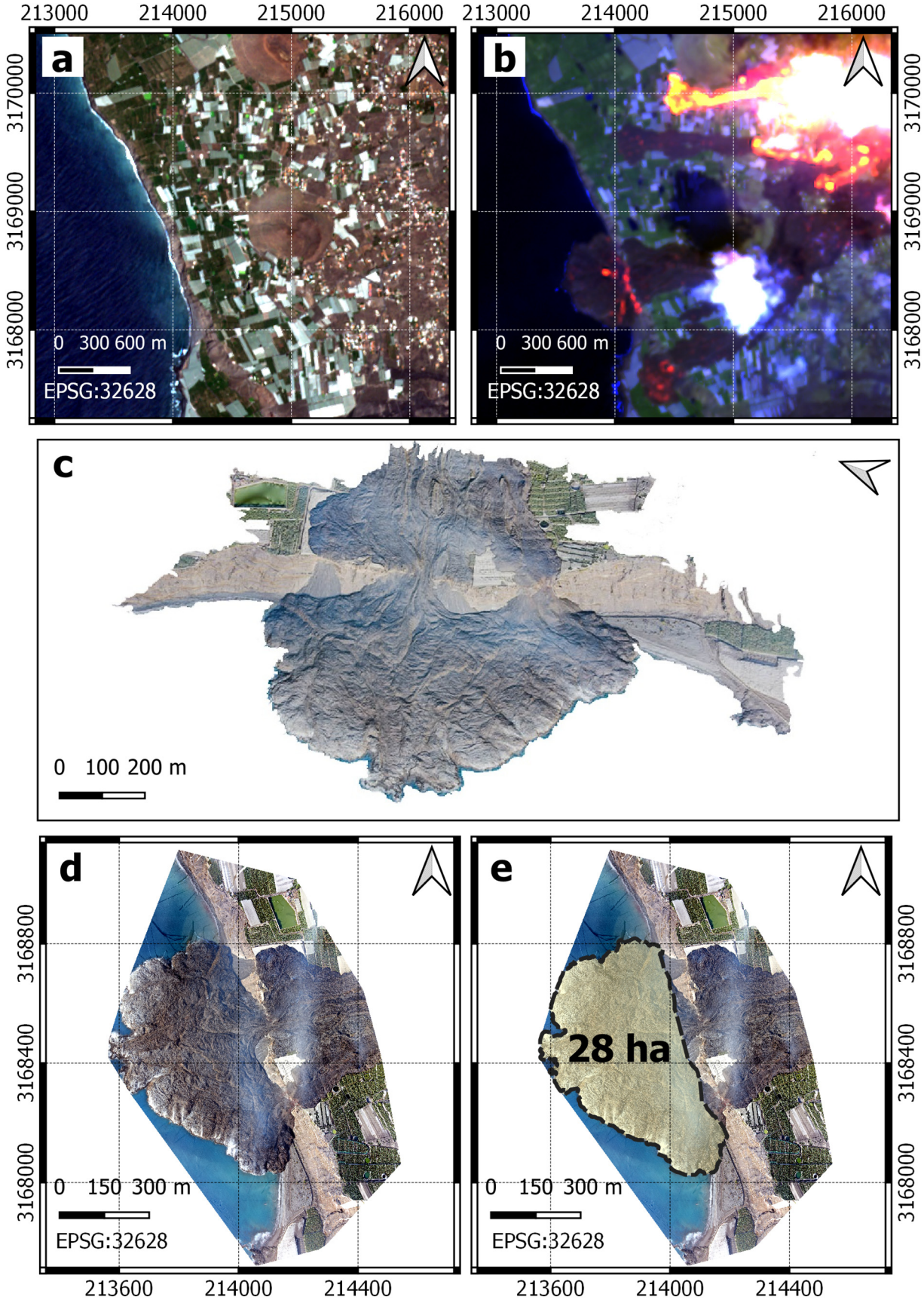

Fig. 4. a) Sentinel-2 level 2A true color composite (bands 4, 3, 2) from September 10th 2021 (pre-eruption); b) Sentinel-2 level 2A false color (urban) composite (bands 12, 11, 4) from October 15th 2021 (post-eruption). Topographic models generated with the SfM workflow followed for the DJI Mavic 2 Pro flight performed on October 2nd 2021 at constant 300 m altitude over the lava delta: c) 3D model; d) optical RGB orthomosaic of the lava delta; e) area of the lava delta in hectares measured over the optical RGB orthomosaic. The QGIS software (v.3.16.14, https://qgis.org/downloads/) was used to create the figures.

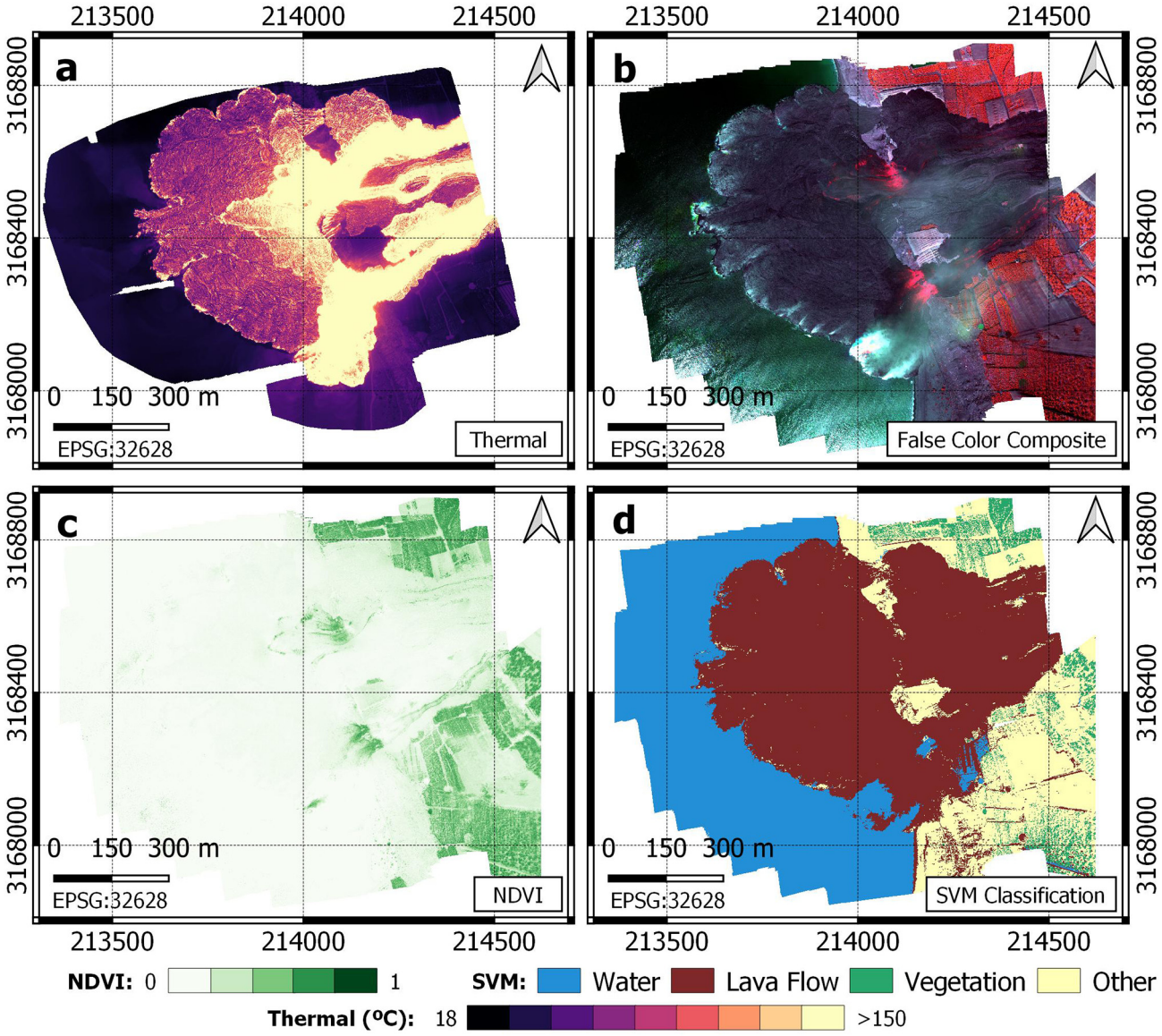

Fig. 5. Topographic models generated with the SfM workflow followed for the Condor hexacopter flight performed on October 2nd 2021 at constant 300 m altitude over the lava delta: a) thermal orthomosaic (relative temperature); b) false color composite (NIR-green-red bands); c) NDVI index; and d) SVM classification. The QGIS (v.3.16.14, https://qgis.org/downloads/) and SAGA GIS (v.7.9.0, https://saga-gis.sourceforge.io/en/index.html) programmes were used to create the figures.

highlighted the volcanic influence on ocean chemistry since these large variations in temperature and salinity are atypical in the ocean.

Table 1 summarizes the values of carbon system parameters and total dissolved nitrogen in surface waters closed to the lava delta, where Blank represents values found at a reference station located 600 m away from the lava delta and, therefore, unaffected by the lava cascade. In this latter case, pH_T and pCO_2 values that are referred to as *in-situ* conditions throughout the text, along with total alcalinity (TA) values, were similar to those typically observed in the Canary basin (González-Dávila et al., 2006). In contrast, surface seawater chemistry around the lava delta was highly altered, with pH_T and TA values decreasing in all the sampled sites with respect to those measured in the remote station. In particular, pH_T ranged from 7.8896 in D4 to 7.2473 in D6, with this latter station and D2 exhibiting pH_T values that were 0.7 and 0.57 units lower than the pH_T in the unaffected area (7.9516). This was also the trend encountered for the TA, as this variable diminished in the surroundings of the lava delta with respect to the TA measured in the control station (2400 μmol/kg). The TA drop was especially evident in D2 and D6, with values nearly 400 μmol/kg lower than that in the Blank station. Moreover, estimated pCO_2 in surface of this reference point was 530 μatm whereas the surface seawater in the sampled sites had pCO_2 values in the range of 595 to 2638 atm, indicating a strong gas oversaturation with respect to the atmospheric CO_2 level in the proximities of the lava cascade.

In addition, dissolved organic carbon (DOC) levels in the transect D1-D2, corresponding to the active front of the lava flow, were much lower (nearly half) than those obtained in the rest of stations and in the control station, which showed very similar concentrations. The lowest DOC values found could be attributed to instant and rapid thermal degradation in the proximities of the lava front. Similarly, levels of total dissolved nitrogen (TDN) were higher in the affected zone compared to those measured in the remote station. This trend could be linked to the inorganic nutrient enrichment normally associated to volcanic emissions that rapidly introduce nitrogen compounds into the water column although this assumption remains to be tested (Hawkes et al., 2015).

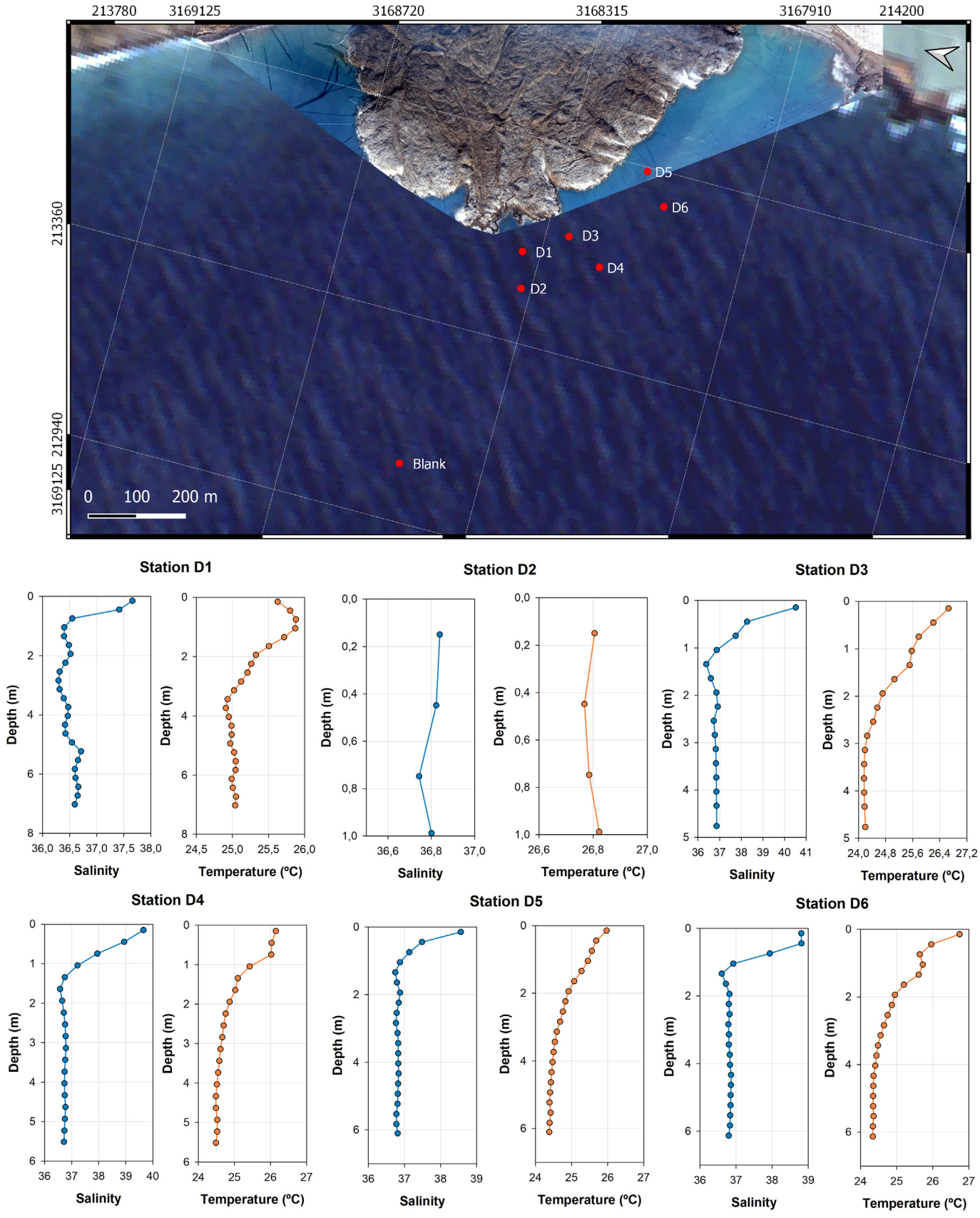

Fig. 6. Vertical profiles of temperature (red line) and salinity (blue line) from the surface to 7 m depth in each sampling station (D1 to D6).

Table 1
Values for the carbonate system measured in surface waters in the six sites (D1-D6) sampled with the Condor hexacopter on October 2nd 2021 (pH, total alkalinity (TA), pCO_2, dissolved organic carbon (DOC) and total dissolved nitrogen (TDN)). For comparative purposes, data obtained in surface waters of a reference station unaffected by the lava delta (Blank) are also indicated. Water sampling locations are shown in Fig. A (see the Supplementary file section).

Station	Ph_T (Ph units)	TA (μmol/kg)	pCO_2 (μatm)	DOC (μmol/L)	TDN (μmol/L)
D1	7.7711	2.256	809	91.52	12.40
D2	7.3861	2.036	1938	115.17	10.75
D3	7.8204	2.260	703	172.59	9.67
D4	7.8896	2.311	596	175.06	9.95
D5	7.7759	2.249	792	162.50	11.30
D6	7.2473	1.995	2538	131.49	11.54
Blank	7.9516	2.403	530	177.58	7.69

4. Discussion

4.1. UAVs for volcanic eruption monitoring

UAV mapping and characterization of natural disasters such as the volcanic eruption described in this study are becoming increasingly common (Dietterich et al., 2017; James et al., 2020; Turner et al., 2017; Walter et al., 2020). On the ground, difficult working conditions are a challenge for data collection, since it is difficult to access the site where the phenomenon is taking place on foot, due to the risk that this entails (Pering et al., 2020; James et al., 2020). The use of UAVs provides a wide range of possibilities to monitor volcanic eruptions during the volcanic crisis, being a simple, low-cost and very safe technique for close-range studies (Giordan et al., 2018; Gomez and Purdie, 2016; Turner et al., 2017). Despite the advantages that UAVs offer for their application in volcanic events (as a feasible, rapid and accurate technique), there are still some limitations mainly related to extreme conditions: i) the air suspended ash and pyroclasts expelled by the volcano can infiltrate the UAV rotors and affect their operation; ii) the high temperatures and hot gases emitted by lava flow can damage equipment and limit flight heights; iii) the risk of losing sight of the UAV, as the large ash-rich plume greatly restrict visibility; iv) the high-temperature and high-speed air currents generated by the volcano make UAV piloting very difficult, increasing the risk of equipment loss or falls; and v) battery life substantially limits data acquisition, as extremely hot weather conditions affect battery performance.

4.2. UAV photogrammetric performance

High-resolution DEMs, 3D models and orthomosaics derived from optical RGB, thermal, and multispectral UAV surveys were particularly valuable for their use during the eruption period, since they allowed us to obtain some useful parameters for lava flow modeling and forecasting, morphological features of the volcanic edifice, and information about the characteristics of the lava delta generated on the coast. In this case study, UAV photogrammetric flights allowed us to generate centimetric orthomosaics and DEMs (maximum spatial resolution of 25.2 cm/pixel and 15 cm for orthomosaics and DEMs, respectively). The use of UAV photogrammetry in active volcanoes has already been tested previously. Favalli et al. (2018) used a hexacopter UAV equipped with a 16-megapixel optical camera to generate a 20 cm DEM for the monitoring of the entire lava flow field of Etna's 1974 eruption. Walter et al. (2020) generated a 20 cm DEM and 10 cm/pixel orthomosaics from a quadcopter UAV equipped with a 20-megapixel optical camera, for the study of the Ebeko volcano (Russia) morphology and characteristics. The results obtained in these studies showed that the use of this tool for monitoring active volcanoes in the future is effective.

These products have facilitated the analysis of the surface morphology of the rubbly and steep terrain after the passage of the lava (Fig. 2), including the distinction between the two types of lava flows (Pahoehoe and A'a) documented by the Spanish National Geographic Institute (IGN, 2021) during the La Palma eruption. In addition, the topographic elevation and slope models derived from the DEMs have made it possible for us to obtain some useful parameters for lava flow modeling, allowing us to identify the most likely routes for the lava flow derived from the eruption. A simple probabilistic model (Q-LavHA) was performed in order to predict the areas with the highest probability of flooding by the lava closest to the vent region. The results obtained (Fig. 3) show a satisfactory coincidence of >70 % between the real data and the modeled, where the predicted final length is approximately 440 m, which is a 50 m underestimation of the real length. The effectiveness of the simulation carried out in this study highlights its value for crisis management, being extremely useful in areas through which the lava has not yet flowed and which are likely to be affected. In addition, there are more complex models that use a greater number of parameters that can be measured *in-situ* or with UAVs, such as the computational fluid dynamic models (VolcFlow, OpenFOAM, FLOW-3D, COMSOL and MOLASSES) used by Dietterich et al. (2017) for lava flow emplacement, or the lava flow propagation models tested by deGraffernried et al. (2021) on a surface crust in the 2018 Lower East Rift Zone (LERZ) eruption at Kilauea (Hawai'i), based on bulk viscosity, yield strength and lava flow growth. Innovations in UAV technology make it possible to measure fundamental parameters such as the effusion rate, considered essential to approach a credible prediction of lava flow (Dietterich et al., 2017).

The generated optical RGB orthomosaics (Fig. 4d–e) have also allowed the calculation of the area occupied by the lava delta formed over the ocean (28 ha on October 2nd 2021, until 43 ha reached by the end of the eruption), which was critical for the analysis of the geographical changes in the extension of the island as well as the quantification of the impact on the marine environment. The high-resolution 3D models of the volcano crater (Fig. 2f) and the lava delta (Fig. 4c) also provided a unique opportunity for mapping and quantifying topographic changes associated with the deformation of the terrain, the accumulation of volcanic material or the mass movements. The thermal structure of the lava delta was characterized with a thermal sensor onboard the UAV (Fig. 5a), capable of generating high resolution thermal orthomosaics (in the order of cm), which are useful for the detection of thermal anomalies and different elements on the ground. Furthermore, high resolution multispectral orthomosaics contributed towards the analysis of the agricultural production areas (mainly banana plantations) strongly affected by the volcano. The false color composite (Fig. 5b), the NDVI index (Fig. 5c) and the supervised classification (Fig. 5d) facilitated identification of the exact distribution of the different elements on the ground, as some of them were undetectable with an optical RGB composite.

4.3. UAV water sampling near the lava delta

The use of the surface water sampling device facilitated collection of crucial information about physical and chemical changes in the marine environment when the lava front reached the coastal zone and entered the water column. Variations in water surface temperature, salinity, total alkalinity, pH and concentrations of dissolved compounds, such as organic carbon and total dissolved nitrogen, were detected compared to measurements taken in a zone unaffected by the lava cascade. The obtained data showed an important increase in temperature and salinity in surface waters close to the lava delta, which could produce certain local alterations on the marine environment. In addition, changes in seawater properties were diagnosed associated with the introduction of the lava into the water column. The observed variations in pH_T in the proximities of the lava delta could be attributed to the entry of gases, such as CO_2, SO_2 and H_2S/HS_2 present in the volcanic fluid, triggering various chemical reactions affecting seawater pH, as reported earlier (Santana-Casiano et al., 2013). In addition, volcanic inputs into the marine environment have been observed to diminish TA in response to mineral alkalinity species and derived reactions inside the lava fluid in contact with seawater (Santana-Casiano et al., 2013). As a result of the chemical alterations in the zone proximal to the lava cascade, a high CO_2 content was detected in surface waters, which was outgassed to

the atmosphere where the CO_2 level was much lower. The TDN values obtained are higher than those measured at the control station, and could be associated with the heating of the colder nitrate-rich mesopelagic waters due to contact with the molten lava flow, which rises to the ocean surface. This inorganic nutrient enrichment of surface waters could fertilize existing algae and favor biological production, as suggested by Hawco et al. (2020) and Wilson et al. (2019), although they might require more days to respond in terms of chlorophyll and growth as in the first hours to few days. In fact, Caballero et al. (2022) confirms that, with Sentinel-2 and Landsat-8 satellites, no substantial increases in chlorophyll-a concentrations or peaked plankton blooms were observed around the lava delta during the volcanic eruption period on La Palma. Nevertheless, other studies suggest that an increase in the occurrence of phytoplankton blooms could occur after extreme weather events or natural disasters such as a volcanic eruption (Lebrato et al., 2019), so this increase in TDN concentrations measured in surface waters near the lava delta could translate into an increase in biological activity in the future. This study highlights the potential of UAVs to obtain valuable measurements of biogeochemical parameters in inaccessible areas that pose a safety risk, allowing operators to maintain a safe distance.

4.4. UAV technology for hazard assessment during the volcanic event

During a volcanic eruption, traditional ground surveys are limited (and mainly restricted) due to the danger of operating in the vicinity of fissures through which magma emanates, in areas affected by the ash column or near the lava flow front (Favalli et al., 2018; Turner et al., 2017). Although surveys in the vicinity of active volcanoes are problematic, data collection is possible with efficient and robust flight planning, considering the flight restrictions established in emergency situations (Favalli et al., 2018). The added value of using UAVs during volcanic eruptions lies not only in the possibility of obtaining high-resolution data for scientific research, but also to generate data products in real time to support crisis management (*e.g.* video footage (see Supplementary Movie 1 file) or high-resolution optical orthomosaics and DEMs produced in short time intervals (from minutes to a few hours). Our study shows that the nearest areas to the vent region, lava flow front or lava delta can be monitored every 1–2 h, offering valuable information from an active site to advise civil protection authorities and the population living in risk areas. The use of models for lava flow forecasting from detailed UAV measurements of lava flow inflation rates, flow thickness, volumetric flow rates or features characterization, are very useful for the evacuation of areas with a high probability of being affected by lava flow, improving emergency response efforts (Turner et al., 2017). In addition, the possibility of mapping with hourly-to-daily DEMs the distribution, morphology or extension of fractures and other volcanic features, could reveal the existence of well-fed lava tubes within the lava flow field and their emission points (Duncan et al., 2004; Favalli et al., 2018). UAV data processing time is low enough to ensure fast response with high spatial resolution data, thus facilitating emergency planning and providing updates on a regular basis. The information derived from machine learning allows us to extract and transfer the most relevant data during flights (*e.g.* classifying and detecting lava flow or hectares of affected vegetation).

The toxic column of water vapor, hydrochloric acid and other gases resulting from seawater and lava interaction on the coast, forces the authorities to establish a security perimeter of 500 m for navigation. The use of UAVs allows us take water samples in areas close to the lava delta, in order to assess the impact of the volcano on the chemistry of the marine environment. UAVs can also be equipped with a gas sampler, although not used in this case study, in order to measure the concentration of harmful gases generated in the lava delta (Mason et al., 2021; Rüdiger et al., 2018). In addition, measuring these gas concentrations could represent a precise approach to climate research, especially in the short term, since the toxic column of water vapor could represent a direct external disturbance on the sensitivity of nature (Kondratyev and Varotsos, 1995; Lovejoy and Varotsos, 2016).

Although previous studies have evaluated the effect of volcanic events on the marine environment through other remote sensing tools, such as satellites (Eugenio et al., 2012; Caballero et al., 2022; Coca et al., 2014), UAVs allow us to deal with satellite limitations such as the presence of clouds and volcanic ash coverage, in order to obtain high-resolution data in near real time without depending on the revisit of the satellite. Remote sensing techniques can be a complementary, synoptic and powerful tool for emergency teams during volcanic eruptions, so that remote sensing-derived data can be easily used in tandem with ground-based measurements, allowing the phenomena to be covered from a broader point of view and facilitating the prevention work for the emergency teams.

5. Conclusions

Overall, the advantages of using UAVs to monitor and manage the evolution of volcanic eruptions outweigh the disadvantages. All the advantages of this methodology are applicable in real time for other natural disasters, such as wildfires, floods or earthquakes, as the UAV offers flexibility that is not offered by other remote or *in-situ* methodologies due to the logistical difficulties associated with these natural phenomena. The volcanic eruption of La Palma is a clear example of the complexity of these natural disasters, where UAVs substantially contributed to providing information based on data obtained with optical RGB, multispectral and thermal sensors, and biogeochemical surface water data collected from a water sampling device, allowing accurate elaboration of orthomosaics, digital elevation models (DEMs), 3D models, probabilistic models of lava flow flooding, or analysis of the chemical composition of surface seawater. In addition, these devices provide real-time data and allow access to highly dangerous restricted areas, providing crucial information for scientists and managers in their assessment of the situation and facilitating the evacuation of populated areas or evaluation of possible impacts of natural disasters of these magnitudes.

Supplementary data to this article can be found online at https://doi.org/10.1016/j.scitotenv.2022.157092.

CRediT authorship contribution statement

All authors contributed to the writing of the manuscript. A. R., A. T-S., D. R-A., and G.N. carried out the UAV flights, collecting thermal, optical and multispectral data, and surface water samples. I. E. H. and E. F-N., analyzed the surface water samples obtained during the campaign. I. C. prepared all Sentinel-2 data and figures.

Funding

This research was funded by grants 20223PAL004 funded by CSIC, and EQC2018-004275-P, EQC2019-005721, RTI2018-098784-J-I00 and IJC2019-039382-I funded by the MCIN/AEI/10.13039/501100011033 and by "ERDF A way of making Europe". A. Román is supported by grant FPU19/04557 funded by Ministry of Universities of the Spanish Government. Data at sea were collected in the context of the VULCANA-III (IEO-2021-2023) project funded by the IEO-CSIC and 20223PAL005 project funded by the Ministry of Science and Innovation of the Spanish Government. This work represents a contribution to CSIC Thematic Interdisciplinary Platforms WATER:iOS and PTI TELEDETECT.

Declaration of competing interest

The authors declare that they have no known competing financial interests or personal relationships that could have appeared to influence the work reported in this paper.

Acknowledgements

This research was funded by grants 20223PAL004 funded by CSIC, and EQC2018-004275-P, EQC2019-005721, RTI2018-098784-J-I00 and IJC2019-039382-I funded by the MCIN/AEI/10.13039/501100011033

and by "ERDF A way of making Europe". A. Román is supported by grant FPU19/04557 funded by Ministry of Universities of the Spanish Government. Data at sea were collected in the context of the VULCANA-III (IEO-2021-2023) project funded by the IEO-CSIC and 20223PAL005 project funded by the Ministry of Science and Innovation of the Spanish Government. This work represents a contribution to CSIC Thematic Interdisciplinary Platforms WATER:iOS and PTI TELEDETECT.

References

Adriano, B., Xia, J., Baier, G., Yokoya, N., Koshimura, S., 2019. Multi-source data fusion based on ensemble learning for rapid building damage mapping during the 2018 Sulawesi earthquake and tsunami in Palu,Indonesia. Remote Sens. 11 (7), 886.

Andaru, R., Rau, J., Syahbana, D.K., Prayoga, A.S., Purnamasari, H.D., 2021. The use of UAV remote sensing for observing lava dome emplacement and areas of potential lahar hazards: an example from the 2017–2019 eruption crisis at Mount Agung in Bali. J. Volcanol. Geotherm. Res. 415, 107255.

Ban, Y., Zhang, P., Nascetti, A., Bevington, A.R., Wulder, M.A., 2020. Near real-time wildfire progression monitoring with Sentinel-1 SAR time series and deep learning. Sci. Rep. 10, 1322.

Bell, A.F., La Femina, P.C., Ruiz, M., Amelung, F., Bagnardi, M., Bean, C.J., Bernard, B., Ebinger, C., Gleeson, M., Grannell, J., Hernandez, S., Higgins, M., Liorzou, C., Lungdren, P., Meier, N.J., Mollhoff, M., Oliva, S., Gorki, A., Stock, M.J., 2021. Caldera resurgence during the 2018 eruption of Sierra Negra volcano,Galápagos Islands. Nat. Commun. 12, 1397.

Bessis, J.L., Bequignon, J., Mahmond, A., 2004. The International Charter 'Space and Major Disasters' initiative. Acta Astronaut. 54 (3), 183–190.

Bonali, F.L., Tibakli, A., Marchese, F., Fallati, L., Russo, E., Corselli, C., Savini, A., 2019. UAV-based surveying in volcano-tectonics: an example from the Iceland rift. J. Struct. Geol. 121, 46–64.

Borgeaud, C., Drinkwater, M., Sivestrin, P., Rast, M., 2015. Status of the ESA earth explorer missions and the new ESA earth observation science strategy. IEEE Int. Geosci. Remote Sens. Symp. 4189–4192.

Bosman, A., Casalbore, D., Romagnoli, C., Chiocci, F.L., 2014. Formation of an 'a'a lava delta: insights from time-lapse multibeam bathymetry and direct observations during the Stromboli 2007 eruption. Bull. Volcanol. 76 (7), 838.

Caballero, I., Fernández, R., Moreno, O., Mamán, L., Navarro, G., 2020. New capabilities of Sentinel-2A/B satellites combined with in situ data for monitoring small harmful algal blooms in complex coastal waters. Sci. Rep. 10, 8743.

Caballero, I., Román, A., Tovar-Sánchez, A., Navarro, G., 2022. Water quality monitoring with Sentinel-2 and Landsat-8 satellites during the 2021 volcanic eruption in La Palma (Canary Islands). Sci. Total Environ. 822, 153433.

Coca, J., Ohde, T., Redondo, A., García-Weil, L., Santana-Casiano, M., González-Dávila, M., Arístegui, J., Fraile-Nuez, E., Ramos, A.G., 2014. Remote sensing of the El Hierro submarine volcanic eruption plume. Int. J. Remote Sens. 35 (17), 6573–6598.

Colson, D., Petropoulos, G.P., Ferentinos, K.P., 2018. Exploring the potential of Sentinels-1 & 2 of the Copernicus mission in support of rapid and cost-effective wildfire assessment. Int. J. Appl. Earth Obs. Geoinf. 73, 262–276.

Conrad, O., Bechtel, B., Bock, M., Dietrich, H., Fischer, E., Gerlitz, L., Wehberg, J., Wichmann, V., Bïhner, J., 2015. System for Automated Geoscientific Analyses (SAGA) v. 2.1.4. Geosci. Model Dev. 8, 1991–2007.

Copernicus Emergency Management Service, n.d.Copernicus Emergency Management Service, n.d. Retrieved October 8th, 2021 from https://emergency.copernicus.eu/.

Council of La Palma, n.d.Council of La Palma, n.d. Retrieved November 9, 2021 from https://www.cabildodelapalma.es/es.

Cracknell, A.P., Varotsos, C.A., 2011. New aspects of global climate-dynamics research and remote sensing. Int. J. Remote Sens. 32 (3), 579–600.

Darmawan, H., Walter, T.R., Brotopuspito, K.S., Subandriyo, Nandaka, I., 2018. Morphological and structural changes at the Merapi lava dome monitored in 2012-15 using unmanned aerial vehicles (UAVs). J. Volcanol. Geotherm. Res. 349, 256–267.

DeGraffenried, R., Hammer, J., Dietterich, H., Perroy, R., Patrick, M., Shea, T., 2021. Evaluating lava flow propagation models with a case study from the 2018 eruption of Kilauea Volcano,Hawai'i. Bull. Volcanol. 83, 65.

Del Valls, T.A., Dickson, A.G., 1998. The pH of buffers based on 2-amino-2 hydroxymethyl-1, 3-propanediol ("tris") in synthetic sea water. Deep-Sea Res. I 45, 1541–1554.

DeVries, B., Huang, C., Armston, J., Huang, W., Jones, J.W., Lang, M.W., 2020. Rapid and robust monitoring of flood events using Sentinel-1 and Landsat data on the Google Earth Engine. Remote Sens. Environ. 240, 111664.

Di Traglia, F., Nolesini, T., Solari, L., Ciampalini, A., Frodella, W., Steri, D., Allotta, B., Rindi, A., Marini, L., Monni, N., Galardi, E., Casagli, N., 2018. Lava delta deformation as a proxy for submarine slope instability. Earth Planet. Sci. Lett. 488, 46–58.

Dickson, A.G., Millero, F.J., 1987. A comparion of the equilibrium constants for the dissociation of carbonic acid in seawater media. Deep-Sea Res. I 34, 1733–1743.

Dietterich, H.R., Lev, E., Chen, J., Richardson, J.A., Cashman, K.V., 2017. Benchmarking computational fluid dynamics models of lava flow simulation for hazard assessment, forecasting, and risk management. J. Appl. Volcanol. 6, 9.

Dou, M., Chen, J., Chen, X., Deng, Z., Zhang, X., Xu, K., Wang, J., 2014. Modeling and simulation for natural disaster contingency planning driven by high-resolution remote sensing images. Future Gener. Comput. Syst. 37, 367–377.

Duncan, A.M., Guest, J.E., Stofan, E.R., Anderson, S.W., Pinkerton, H., Calvari, S., 2004. Development of tumuli in the medial portion of the 1983 aa flow-field, Mount Etna,Sicily. J. Volcanol. Geotherm. Res. 132, 173–187.

ESA, 2015. Sentinel-2 User Handbook. ESA Standard Document Paris, France. https://sentinel.esa.int/documents/247904/685211/Sentinel-2_User_Handbook.

ESA, 2017. Sentinel-2 MSI Technical Guide. https://earth.esa.int/web/sentinel/technicalguides/sentinel-2-msi.

Eugenio, F., Marcello, J., Martin, J., 2012. Monitoring El Hierro submarine volcano with low and high resolution satellite images. Proc. SPIE 8538, 853816-1.

Favalli, M., Fornaciai, A., Nannipieri, L., Harris, A., Calvari, S., Lormand, C., 2018. UAV-based remote sensing surveys of lava flow fields: a case study from Etna's 1974 channel-fed lava flows. Bull. Volcanol. 80, 29.

Felpeto, A., Araña, V., Ortiz, R., Astiz, M., García, A., 2001. Assessment and modelling of lava flow hazard on Lanzarote (Canary Islands). Nat. Hazards 23 (2–3), 247–257.

Fink, J.H., Malin, M.C., Anderson, S.W., 1990. Intrusive and extrusive growth of the Mount St Helens lava dome. Nature 348, 435–437.

Ganci, G., Cappello, A., Bilotta, G., Del Negro, C., 2020. How the variety of satellite remote sensing data over volcanoes can assist hazard monitoring efforts: the 2011 eruption of Nabro volcano. Remote Sens. Environ. 236, 111426.

Giordan, D., Hayakawa, Y., Nex, F., Remondino, F., Tarolli, P., 2018. Review article: the use of remotely piloted aircraft systems (RPASs) for natural hazards monitoring and management. Nat. Hazards Earth Syst. Sci. 18, 1079–1096.

Gomez, C., Purdie, H., 2016. UAV- based photogrammetry and geocomputing for hazards and disaster risk monitoring – a review. Geoenviron.Disasters 3, 23.

González-Dávila, M., Santana-Casiano, J.M., de Armas, D., Escánez, J., Suarez-Tangil, M., 2006. The influence of island generated eddies on the carbon dioxide system, south of the Canary Islands. Mar. Chem. 99, 177–190.

Gray, D.M., Burton-Johnson, A., Fretwell, P.T., 2019. Evidence for a lava lake on Mt. Michael volcano, Saunders Island (South Sandwich Islands) from Landsat, Sentinel-2 and ASTER satellite imagery. J. Volcanol. Geotherm. Res. 379, 60–71.

Harris, A.J.L., Rowland, S.K., 2001. FLOWGO: a kinematic thermo-rheological model for lava flowing in a channel. Bull. Volcanol. 63, 20–44.

Hawco, N.J., Yang, S.C., Foreman, R.K., Funkey, C.P., Dugenne, M., White, A.E., Wilson, S.T., Kellym, R.L., Bian, X., Huang, K.F., Karl, D.M., John, S.G., 2020. Metal isotope signatures from lava-seawater interaction during the 2018 eruption of Kilauea. Geochim. Cosmochim. Acta 282, 340–356.

Hawkes, J.A., Rossel, P.E., Stubbins, A., Butterfield, D., Connelly, D.P., Achterberg, E.P., Koschinsky, A., Chavagnac, V., Hansen, C.T., Bach, W., Dittmar, T., 2015. Efficient removal of recalcitrant deep-ocean dissolved organic matter during hydrothermal circulation. Nat. Geosci. 8, 856–860.

Hildenbrand, A., Marques, F.O., Catalao, J., Catita, C.M.S., Costa, A.C.G., 2012. Large-scale active slump of the southeastern flank of Pico Island,Azores. Geology 40 (10), 939–942.

IGN, 2021. Informe mensual de vigilancia volcánica. IGN. https://www.ign.es/web/resources/volcanologia/html/CA_noticias.html.

James, M.R., Carr, B.B., D'Arcy, F., Diefenbach, A.K., Dietterich, H.R., Fornaciai, A., Lev, E., Liu, E.J., Pieri, D.C., Rodgers, M., Smets, B., Terada, A., von Aulock, F.W., Walter, T.R., Wood, K.T., Zorn, E.U., 2020. Volcanological applications of unoccupied aircraft systems (UAS): developments, strategies, and future challenges. Volcanica 3 (1), 67–114.

Jelének, J., Kopacková-Strnadová, V., 2021. Synergic use of Sentinel-1 and Sentinel-2 data for automatic detection of earthquake-triggered landscape changes: a case study of the 2016 Kaikoura earthquake (Mw 7.8), New Zealand. Remote Sens. Environ. 265, 112634.

Kaku, K., 2019. Satellite remote sensing for disaster management support: a holistic and staged approach based on case studies in Sentinel Asia. Int. J. Disaster Risk Reduct. 33, 417–432.

Kazahaya, R., Shinohara, H., Ohminato, T., Kaneko, T., 2019. Airborne measurements of volcanic gas composition during unrest at Kuchinoerabujima volcano,Japan. Bull. Volcanol. 81, 7.

Konapala, G., Kumar, S.V., Ahmad, S.K., 2021. Exploring Sentinel-1 and Sentinel. 2 diversity for flood inundation mapping using deep learning. ISPRS J. Photogramm. Remote Sens. 180, 163–173.

Kondratyev, K.Y., Varotsos, C.A., 1995. Volcanic eruptions and global ozone dynamics. Int. J. Remote Sens. 16 (10), 1887–1895.

Krapivin, V.F., Soldatov, V.Y., Varotsos, C.A., Cracknell, A.P., 2012. An adaptive information technology for the operative diagnostics of the tropical cyclones; solar-terrestrial coupling mechanisms. J. Atmos. Sol.-Terr. Phys. 89, 83–89.

Kucharczyk, M., Hugenholtz, C.H., 2021. Remote sensing of natural hazard-related disasters with small drones: global trends, biases, and research opportunities. Remote Sens. Environ. 264, 112577.

Lebrato, M., Wang, Y.V., Tseng, L., Achterberg, E.P., Chen, X., Molinero, J., Bremen, K., Westemströer, U., Söding, E., Dahms, H., Küter, M., Heinath, V., Jöhnck, J., Konstantinou, K.I., Yang, Y.J., Hwang, J., Garbe-Schönberg, D., 2019. Earthquake and typhoon trigger unprecedented transient shifts in shallow hydrothermal vents biogeochemistry. Sci. Rep. 9, 16926.

Lewis, E., Wallace, D., Allison, L.J., 1998. Program Developed for CO2 System Calculations. Carbon Dioxide Information Analysis Center, managed by Lockheed Martin Energy Research Corporation for the US Dep. of Energy, Oak Ridge, Tenn.

Li, Y., Jiang, W., Zhang, J., Li, B., Yan, B., Wang, X., 2021. Sentinel-1 SAR-based coseismic deformation monitoring service for rapid geodetic imaging of global earthquakes. Nat. Hazards Res. 1, 11–19.

Liu, E.J., Wood, K., Mason, E., Edmons, M., Aiuppa, A., Giudice, G., Bitetto, M., Francofonte, V., Burrow, S., Richardson, T., Watson, M., Pering, T.D., Wilkes, T.C., McGonigle, A.J.S., Velasquez, G., Melgarejo, C., Bucarey, C., 2019. Dynamics of Outgassing and Plume Transport Revealed by Proximal Unmanned Aerial System (UAS) Measurements at Volcán Villarrica,Chile. Geochem. Geophys. 20, 730–750.

Llorens, R., Sobrino, J.A., Fernández, C., Fernández-Alonso, J.M., Vega, J.A., 2021. A methodology to estimate forest fires burned areas and burn severity degrees using Sentinel-2 data. Application to the October 2017 fires in the Iberian Peninsula. Int. J. Appl. Earth Obs. Geoinf. 95, 102243.

Lovejoy, S., Varotsos, C., 2016. Scaling regimes and linear/nonlinear responses of last millennium climate to volcanic and solar forcings. Earth Syst. Dynam. 7, 133–150.
Malawani, M.N., Lavigne, F., Gomez, C., Mutaqin, B.W., Hadmoko, D.S., 2021. Review of local and global impacts of volcanic eruptions and disaster management practices: the Indonesian example. Geosci. 11, 109.
Mason, E., Wieser, P.E., Liu, E.J., Edmonds, M., Ilyinskaya, E., Whitty, R.C.W., Mather, T.A., Elias, T., Nadeau, P.A., Wilkes, T.C., McGonigle, A.J.S., Pering, T.D., Mims, F.M., Kern, C., Schneider, D.J., Oppenheimer, C., 2021. Volatile metal emissions from volcanic degassing and lava-seawater interactions at Kilauea VolcanoHawai'i. Commun. Earth Environ. 2 (1), 79.
Mehrbach, C., Culberson, C.H., Hawley, J.E., Pytkowicz, R.M., 1973. Measurement of the apparent dissociation constants of carbonic acid in seawater at atmospheric pressure. Limnol. Oceanogr. 18, 897–907.
Mintrop, L., Pérez, F.F., González-Dávila, M., Santana-Casiano, M.J., Kortzinger, A., 2002. Alkalinity determination by potentiometry: intercalibration using three different methods. Cien. Mar. 26 (1), 23–37.
Miranda, V., Pina, P., Heleno, S., Vieira, G., Mora, C., Schaefer, C.E.G.R., 2020. Monitoring recent changes of vegetation in Fildes Peninsula (King George Island, Antarctica) through satellite imagery guided by UAV surveys. Sci. Total Environ. 704, 135295.
Mori, T., Hashimoto, T., Terada, A., Yoshimoto, M., Kazahaya, R., Shinohara, H., Tanaka, R., 2016. Volcanic plume measurements using a UAV for the 2014 Mt.Ontake eruption. Earth Planets Space 68, 49.
Mueller, C.S., Briggs, R.W., Wesson, R.L., Petersen, M.D., 2015. Updating the USGS seismic hazard maps for Alaska. Quat. Sci. Rev. 113, 39–47.
Ogashawara, I., 2019. The use of Sentinel-3 Imagery to monitor cyanobacterial blooms. Remote Sens. 6, 60.
Pering, T.D., Liu, E.J., Wood, K., Wilkes, T.C., Aiuppa, A., Tamburello, G., Bitetto, M., Richardson, T., McGonigle, A.J.S., 2020. Combined ground and aerial measurements resolve vent-specific gas fluxes from a multi-vent volcano. Nat. Commun. 11, 3039.
Plank, S., Marchese, F., Genzano, N., Nolde, M., Martinis, S., 2020. The short life of the volcanic island New Late'iki (Tonga) analyzed by multi-sensor remote sensing data. Sci. Rep. 10, 22293.
Poland, M.P., Orr, T.R., 2014. Identifying hazards associated with lava deltas. Bull. Volcanol. 76, 880.
Rodríguez-Benito, C.V., Navarro, G., Caballero, I., 2020. Using Copernicus Sentinel-2 and Sentinel-3 data to monitor harmful algal blooms in Southern Chile during the COVID-19 lockdown. Mar. Pollut. Bull. 161, 111722.
Rüdiger, J., Tirpitz, J., de Moor, J.M., Bobrowski, N., Gutmann, A., Liuzzo, M., Ibarra, M., Hoffmann, T., 2018. Implementation of electrochemical, optical and denuder-based sensors and sampling techniques on UAV for volcanic gas measurements: examples from Masaya, Turrialba and Stromboli volcanoes. Atmos. Meas. Tech. 11, 2441–2457.
Salgado, X.A., Miller, A.E.J., 1998. Simultaneous determination of dissolved organic carbon and total dissolved nitrogen in seawater by high temperature catalytic oxidation: conditions for accurate shipboard measurements. Mar. Chem. 62 (3–4), 325–333.
Santana-Casiano, J.M., González-Dávila, M., Fraile-Nuez, E., de Armas, D., González, A.G., Domínguez-Yanes, J.F., Escánez, J., 2013. The natural ocean acidification and fertilization event caused by the submarine eruption of El Hierro. Sci. Rep. 3, 1140.
Solikhin, A., Thouret, J., Gupta, A., Harris, A.J.L., Liew, S.C., 2012. Geology, tectonics, and the 2002–2003 eruption of the Semeru volcano, Indonesia: interpreted from high-spatil resolution satellite imagery. Geomorphology 138, 364–379.
Sparaventi, E., Rodríguez-Romero, A., Navarro, G., Tovar-Sánchez, A., 2022. A novel automatic water autosampler operated from UAVs for determining dissolved trace elements. Front. Mar. Sci. 9, 879953.
Stewart, C., Johnston, D.M., Leonard, G.S., Horwell, C.J., Thordason, T., Cronin, S.J., 2006. Contamination of water supplies by volcanic ashfall: a literature review and simple impact modelling. J. Volcanol. Geotherm. Res. 158, 296–306.
Sukov, A.I., Soldatov, V.Y., Krapivin, V.F., Cracknell, A.P., Varotsos, C.A., 2008. A sequential analysis method for the prediction of tropical hurricanes. Int. J. Remote Sens. 29 (9), 2787–2798.
Terada, A., Morita, Y., Hashimoto, T., Mori, T., Ohba, T., Yaguchi, M., Kanda, W., 2018. Water sampling using a drone at Yugama crater lake, Kusatsu-Shirane volcano,Japan. Earth Planets Space 70, 64.
Tovar-Sánchez, A., Román, A., Roque-Atienza, D., Navarro, G., 2021. Applications of unmanned aerial vehicles in Antarctic environmental research. Sci. Rep. 11, 21717.
Turner, N.R., Perroy, R.L., Hon, K., 2017. Lava flow hazard prediction and monitoring with UAS: a case study from the 2014–2015 Pāhoa lava flow crisis, Hawai'i. J. Appl. Volcanol. 6, 17.
Vapnick, V., 1995. The Nature of Statistical Learning Theory. Springer-Verlag, New York, NY.
Walter, T.R., Belousov, A., Belousova, M., Kotenko, T., Auer, A., 2020. The 2019 eruption dynamics and morphology at Ebeko volcano monitored by unoccupied aircraft systems (UAS) and field stations. Remote Sens. 12, 1961.
Wilson, S.T., Hawco, N.J., Armbrust, E.V., Barone, B., Bjorkman, K.M., Boysen, A.K., Burgos, M., Burrell, T.J., Casey, J.R., DeLong, E.F., Dugenne, M., Dutkiewicz, S., Dyhrman, S.T., Ferrón, S., Follows, M.J., Foreman, R.K., Funkey, C.P., Harke, M.J., Henke, B.A., Hill, C.N., Hynes, A.M., Ingalls, A.E., Jahn, O., Kelly, R.L., Knapp, A.N., Letelier, R.M., Ribalet, F., Shimabukuro, E.M., Tabata, R.K.S., Turk-Kubo, K.A., White, A.E., Zehr, J.P., John, S., Karl, D.M., 2019. Kilauea lava fuels phytoplankton bloom in the North Pacific Ocean. Science 365, 1040–1044.
Yuan, X., Zhang, X., Wang, X., Zhang, Y., 2021. Flood disaster monitoring based on Sentinel-1 data: A case study of Sihu Basin and Huaibei Plain,China. Water Sci. Eng. 14 (2), 87–96.
Zhao, Z., Mitchell, N.C., Quartau, R., Ramalho, R.S., Rusu, L., 2020. Coastal erosion rates of lava deltas around oceanic islands. Geomorphology 370, 107410.
Zorn, E.U., Walter, T.R., Johnson, J.B., Mania, R., 2020. UAS-based tracking of the Santiaguito Lava Dome,Guatemala. Sci. Rep. 10, 8644.